

Heterogeneity in hydrogenated silicon: Evidence for intermediately ordered chainlike objectsDavid V. Tsu, Benjamin S. Chao, Stanford R. Ovshinsky, and Scott J. Jones
*Energy Conversion Devices, Troy, Michigan 48084*Jeffrey Yang and Subhendu Guha
United Solar Systems Corporation, Troy, Michigan 48084

Raphael Tsu

Electrical Engineering Department, University of North Carolina at Charlotte, Charlotte, North Carolina 28223
(Received 23 December 1999; revised manuscript received 6 November 2000; published 13 March 2001)

Hydrogen (H_2) dilution of the source gas is known to be a key factor in producing hydrogenated amorphous silicon films that demonstrate a high degree of optoelectronic stability. In this work, we investigate, using Raman spectroscopy and high-resolution transmission electron microscopy (TEM), whether microstructural differences exist between such films and those made with no H_2 dilution (i.e., that have greater instabilities). The key variable is the H_2 dilution, which ranges from none to very high levels, producing amorphous and microcrystalline silicon films. The TEM results show that embedded within the amorphous matrix are chainlike objects (CLO's) having ~ 3 nm widths, ~ 30 nm lengths, and showing a high degree of order along their length. Such order implies vanishing levels of bond-angle distortion (BAD). These CLO's are present in all samples investigated, but their density increases with the level of H_2 dilution. The Raman spectra show a TO band centered at 490 cm^{-1} ($37 \pm 3\text{ cm}^{-1}$ full width). Quantitative analysis shows this band to exist in *all* samples investigated, but increases in magnitude with increasing H_2 dilution. In the highest dilutions when microcrystallites are observed, the band is distinctly evident. Its position and width are also consistent with very low (crystallinelike) levels of BAD $\sim 0^\circ$. It is thus likely the 490 cm^{-1} Raman band is a signature of the intermediate ordered CLO's.

DOI: 10.1103/PhysRevB.63.125338

PACS number(s): 61.43.-j, 61.43.Dq, 61.44.Br, 61.46.+w

I. INTRODUCTION

The question¹ whether a structural state exists in hydrogenated amorphous silicon ($a\text{-Si:H}$) between the amorphous state of short-range order and the microcrystalline state of long-range order has stimulated renewed interest. This state of intermediate order might be disordered enough to spoil the crystalline selection rules for optical transitions, hence providing for the strong optical absorption desired in photovoltaic devices (e.g., solar cells). It may yet be ordered enough to inhibit any structural changes and photoinduced defects that decrease the photocarrier lifetimes. Such a decrease ultimately leads to reduced efficiencies of these photovoltaic devices during long light exposures. The decrease or elimination of this degradation, which is called the Staebler-Wronski degradation (SWD) after its discoverers,² is one of the major goals in the research of $a\text{-Si:H}$ and related materials.

The understanding of device stability is increasingly being focused on the nature of heterogeneity within the amorphous silicon material.^{3,4} It is now commonly accepted that an early *homogeneous* model⁵ of the amorphous state, based upon the continuous random network (CRN), is inadequate. The difficulty lies in identifying in more precise terms the nature of heterogeneity,³ i.e., how a particular sort of heterogeneity might be favorable to stability. Thus, the issue of an intermediate ordered phase of silicon is centrally connected with gaining a more precise description of heterogeneity.

Experimentally, deposition conditions are being found that result in materials that have substantially lower SWD's. Recently,⁶ a significant reduction of the SWD of $a\text{-Si:H}$ so-

lar cells was accomplished by modifying the plasma-enhanced chemical vapor deposition (PECVD) conditions of the $a\text{-Si:H}$ layers. This modification primarily involved the use of fairly high levels of hydrogen dilution of the disilane (Si_2H_6) process gas. This led to the development of solar cells⁷ with $\sim 15\%$ initial efficiency and with a stabilized efficiency of $\sim 13\%$, representing a degradation of only $\sim 10\%$. The observed improvement of the $a\text{-Si:H}$ material thus motivated us to investigate whether this achievement could be attributed to a more ordered microstructure, i.e., to explore the nature of the heterostructure within this improved material. In particular, we revisit the possible existence of an intermediate ordered phase of silicon⁸⁻¹⁰ being one of the heterogeneous elements.

Early work on the existence of an intermediately ordered state of silicon was based on electroreflectance and Raman spectroscopic analyses⁸⁻¹⁰ of fluorinated amorphous hydrogenated silicon ($a\text{-Si:F:H}$). The electroreflectance data^{8,9} indicated the presence of a structural component that could not be identified with either crystalline or amorphous states, and thus they interpreted that other component to have intermediate range order (IRO). Although a Raman peak at $\sim 508\text{ cm}^{-1}$ was first thought to be a signature of IRO,⁸ transmission electron microscopy (TEM) and electron diffraction analyses⁹ later showed this peak to be associated with very small (2–6 nm) microcrystallites, where small-particle effects cause the measurement of the zone-center phonons to be shifted down from the 522 cm^{-1} value of crystalline silicon.

Raman analysis of the transverse optical (TO) band^{9,10} showed that its peak position and width could be used to

classify the relative order of the amorphous material. The position of the TO Raman band in sputtered amorphous silicon (*a*-Si) shifts from about 465 cm^{-1} to roughly 475 cm^{-1} upon annealing. This peak shift was interpreted to indicate an increase in the local order of the material,¹⁰ as a consequence of a reduction of the average bond-angle deviation (BAD), from the 109.5° of tetrahedral coordination, within the random network. Hydrogenated material (*a*-Si:H) could be deposited directly in the state that results in the 475 cm^{-1} Raman peak, but annealing of *a*-Si:H was shown to be ineffectual in raising the frequency higher than 475 cm^{-1} . Peak positions below 475 cm^{-1} were thus deemed to indicate short-range order. Only by the introduction of fluorine in *a*-Si:F:H alloys could TO peak positions above 475 cm^{-1} be measured. In fact, positions up to 483 cm^{-1} were measured. TO frequencies this high was thought to indicate the existence of IRO.^{9,10}

Since those early studies, Raman spectroscopy has been extensively used to study the quality of microcrystalline silicon (μc -Si).¹¹ It is noteworthy that in addition to the main microcrystalline Raman band, whose peak position can range from 508 to 522 cm^{-1} (depending on the microcrystallite dimension),⁹ a distinct bump on the low-frequency side at $\sim 490\text{ cm}^{-1}$ is generally observed. High-resolution TEM analysis of primarily microcrystalline material was performed by Wang.¹² He makes two conclusions about the 490 cm^{-1} band: (1) it does *not* derive from any amorphous content, and (2) it may be related to the “tissue” between microcrystallites. We believe, however, that this 490 cm^{-1} Raman band is associated with an intermediately ordered phase of silicon.

An intermediately ordered phase of silicon has been implicated in both amorphous and microcrystalline material. To clarify the nature of intermediate order, this paper extends our earlier work,¹³ where we examined only *a*-Si:H. Here, we extend the hydrogen dilution into a regime that also results in μc -Si. Following those earlier studies,^{8–12} we also use the TO Raman peak as a measure of the microstructure as well as TEM and electron diffraction. We will show that the intermediate order, which is clearly evident in the μc -Si material, has its roots in the amorphous material.

II. EXPERIMENTAL DETAILS

The *a*-Si:H films were deposited by PECVD using 13.56-MHz rf power onto Corning 7059 glass substrates at a temperature (T_s) of either 150 or 300°C and at a deposition rate of about 1 \AA/s . The film thickness was close to 50 nm to allow both Raman and TEM measurements on the same sample. In this work, two classes of samples were produced: (1) reference samples prepared using pure silane gas (SiH_4), i.e., without the use of any H_2 dilution, and (2) modified samples prepared with disilane (Si_2H_6) diluted with various amounts of H_2 gas. These samples are listed in Table I. In this table, the undiluted reference samples (i.e., made without H_2 dilution) are indicated as the U_x series, while the H_2 diluted samples made at the higher and lower substrate temperatures are labeled as DH_x and DL_x , respectively. Also, while the U_x series was made with silane, and the DH_x and

TABLE I. Summary of samples investigated. All samples are $\sim 50\text{ nm}$ thick, except sample U_1 , which is $\sim 500\text{ nm}$ thick. The H_2 dilution factor is defined as $(\text{H}_2 + \text{Si}_2\text{H}_6)/\text{Si}_2\text{H}_6$.

Sample name	Gas	H_2 dilution	T_s ($^\circ\text{C}$)
U_1	SiH_4	1	300
U_2	SiH_4	1	300
U_3	SiH_4	1	300
U_4	SiH_4	1	300
DH_1	$\text{Si}_2\text{H}_6 + \text{H}_2$	Low	300
DH_2	$\text{Si}_2\text{H}_6 + \text{H}_2$	Medium	300
DH_3	$\text{Si}_2\text{H}_6 + \text{H}_2$	High	300
DL_4	$\text{Si}_2\text{H}_6 + \text{H}_2$	250	150
DL_5	$\text{Si}_2\text{H}_6 + \text{H}_2$	285	150
DL_6	$\text{Si}_2\text{H}_6 + \text{H}_2$	330	150
DL_7	$\text{Si}_2\text{H}_6 + \text{H}_2$	400	150
DL_8	$\text{Si}_2\text{H}_6 + \text{H}_2$	500	150

DL_x samples made with disilane, this difference is not expected to be significant.

For TEM and the selected-area transmission electron diffraction (TED) studies, the *a*-Si:H films were lifted from their glass substrates by first scoring, then etching in a weak HF solution. The films were then floated onto a thin copper TEM grid. Planar images were taken with a Jeol 2010 scanning TEM, operating at 200 keV . In this way, the films were subjected to a minimum amount of preparation.

Raman spectra were collected in the near-backscattering geometry using the 488 nm line of an Ar-ion laser at 300 mW . A cylindrical lens focused the laser light into a line that matches the entrance slit of the double monochromator (Spex model 1403, 0.85 m). The laser plasma lines were unfiltered so that their positions could be used to accurately calibrate the absolute Raman shifts. Detection is by a thermoelectrically cooled photomultiplier having about 4 dark counts/s. Scans were made between 400 and 580 cm^{-1} at slow scan rates ($0.01\text{ cm}^{-1}/\text{s}$) and long integration times (10 s) to obtain high signal-to-noise ratio spectra.

III. EXPERIMENTAL RESULTS

A. High-resolution

Figures 1(a) and 1(b) are the TEM bright-field and dark-field photographs of sample DH_3 in relatively low magnification. One observes a gross microstructure consisting of microcrystalline inclusions embedded in an amorphous matrix. The microcrystalline inclusions typically have a diameter of $\sim 30\text{--}50\text{ nm}$ and are conglomerations of smaller microcrystallites that range from 2.5 to 10 nm in diameter, as shown in the corresponding dark-field micrograph of Fig. 1(b). The heterogeneous nature of this sample is further revealed by the TED pattern shown in Fig. 1(c). Here, we note two distinct halos that result from the amorphous regions, as well as small bright diffraction spots. The diffraction spots are found in three distinct locations: (1) within the boundaries of the first inner halo, and (2) on the inner and (3) outer

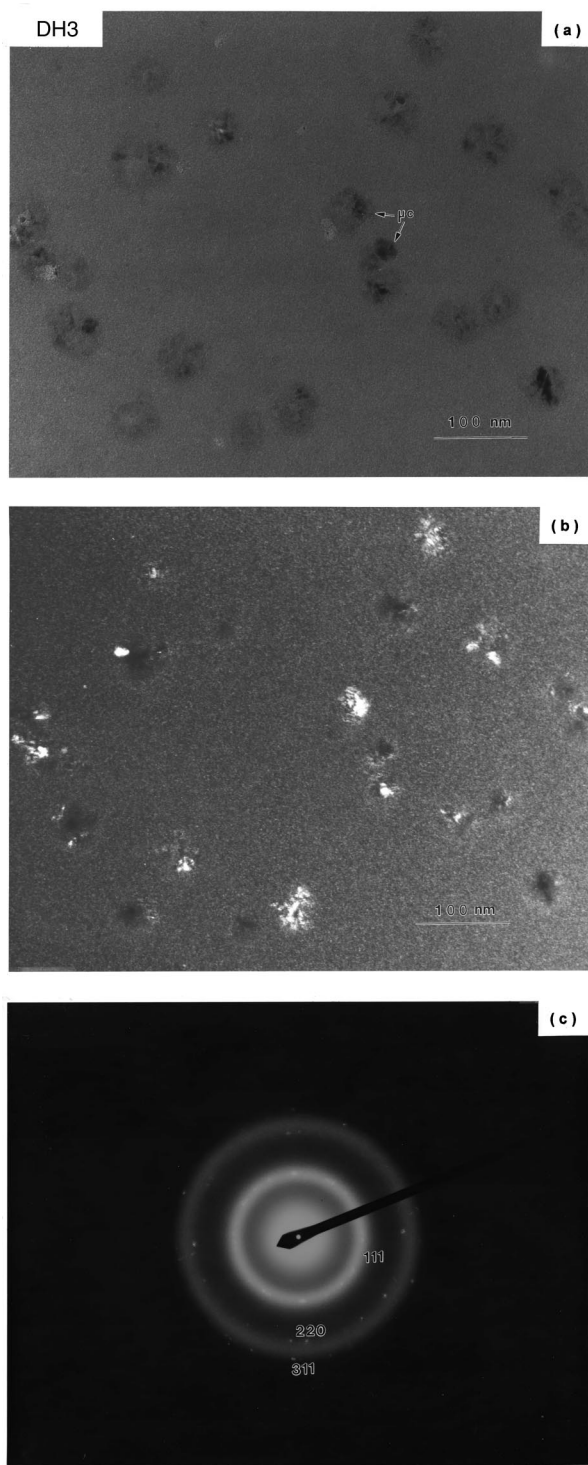


FIG. 1. Low magnification planar TEM of sample DH3 showing the (a) bright-field and (b) dark-field micrographs and (c) the corresponding TED pattern.

edges of the second halo. These correspond to the (111), (220), and (311) diffraction planes of crystalline Si, respectively. The well-defined splitting on the (220) and (311) diffraction rings indicates that the microcrystallites possess long-range order. No such diffraction spots are found in the undiluted reference samples (U1–U4) nor in the samples modified with lower levels of H_2 dilution (DH1 and DH2).

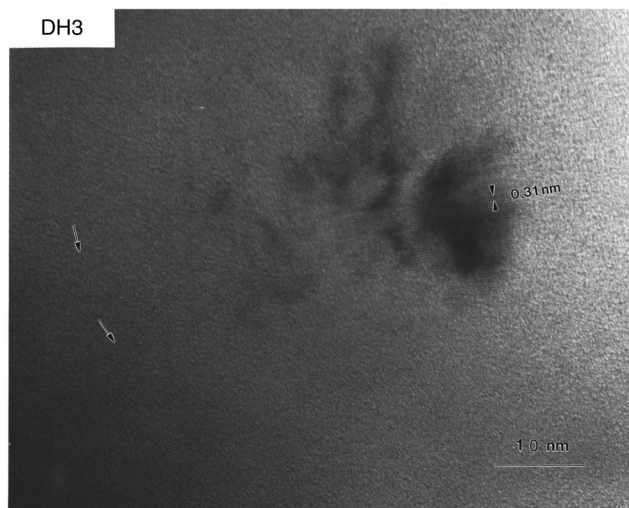


FIG. 2. High-magnification bright-field TEM of one of the microcrystallites seen in Fig. 1.

One of the microcrystallites imbedded in the amorphous matrix is shown in the bright-field micrograph of Fig. 2. The long parallel lines separated by 0.31 nm correspond to the spacing of Si(111) planes. Aside from the microcrystallites, one observes that the amorphous matrix is not entirely featureless. As indicated by the arrows, one finds meandering structures that we call “chainlike objects” (CLO’s) that are quasi-one-dimensional, having widths of 2–3 nm (~ 10 Si atoms) and lengths up to 30 nm, which have a rather high degree of order along their length as evidenced by the short (~ 2 nm) repeating segments perpendicular to the length of the CLO’s, e.g., like III . . . III. Although the precise nature of this order cannot be discerned from these images, it is clear that they must consist of bonding units having very small deviations from the ideal angle of 109.5° of tetrahedral coordination. For even minor deviations from this ideal angle must destroy this observed regularity. It is known that an average BAD of $\sim 10^\circ$ exists in well annealed *random* networks and that BAD accounts for virtually all of the elevated strain energy found in amorphous silicon networks. These objects, then, must represent *local* regions having substantially reduced internal strain in comparison to the surrounding random network. Thus, an important property that the CLO’s conveys onto the heterogeneous material is to introduce local regions having very low strain energy. Moreover, this sort of heterogeneity, i.e., between the CRN amorphous matrix and the meandering CLO’s, should have beneficial interfacial qualities in comparison to the interface between rigid microcrystallites and the CRN matrix.

Figure 3 is a closeup view of one of these chainlike objects. They appear to meander throughout the matrix in no particular direction. Some CLO’s are also found in the reference samples (U1–U4) prepared without any H_2 dilution. However, their concentration increases with an increase in the level of H_2 dilution in the process gas. Such structures have also recently been identified in *a*-Si:H by Kamei, Stradins, and Matsuda.¹⁴ The concentration of the microcrystallites also increases with H_2 dilution, but becomes noticeable only in the very-high-dilution regime.

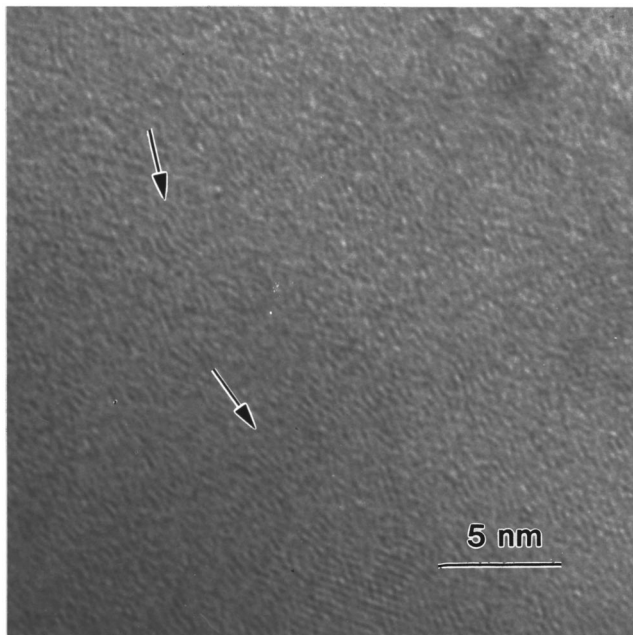


FIG. 3. High magnification of the “featureless amorphous region” (as seen in the low-magnification image of Fig. 1) away from the microcrystallites. The chainlike objects are meandering across this planar image.

B. Raman spectra

Figure 4 shows the Raman spectra (a) of an undiluted reference sample (U3) and traces (b)–(d) are of the H₂ diluted samples DH1, DH2, and DH3, respectively. All of the spectra were normalized with respect to the baseline near $\nu = 560 \text{ cm}^{-1}$ and the peak of the longitudinal optical (LO) band near $\nu = 400 \text{ cm}^{-1}$. With increasing H₂ dilution, the peak position of the TO band increases from 475 to 482.6 cm^{-1} as shown by the dashed line in the figure. The narrow band in trace (d) at 516.5 cm^{-1} is due to microcrystalline inclusions as confirmed by TEM and shown in Fig. 1(a). The

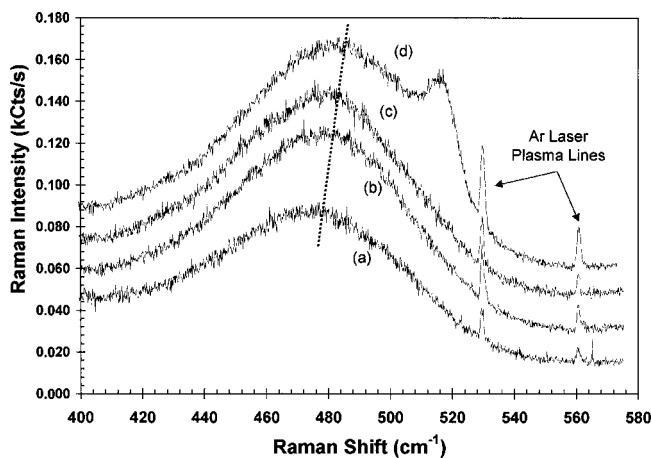


FIG. 4. Raman spectra vs H₂ dilution of the process gas of $\sim 50\text{-nm}$ films on 7059 Corning glass: (a) U3 $s(\times 1.0)$, no dilution; (b) DH1 ($\times 0.68$), low dilution; (c) DH2 ($\times 1.05$), medium dilution; and (d) DH3 ($\times 0.55$), high dilution.

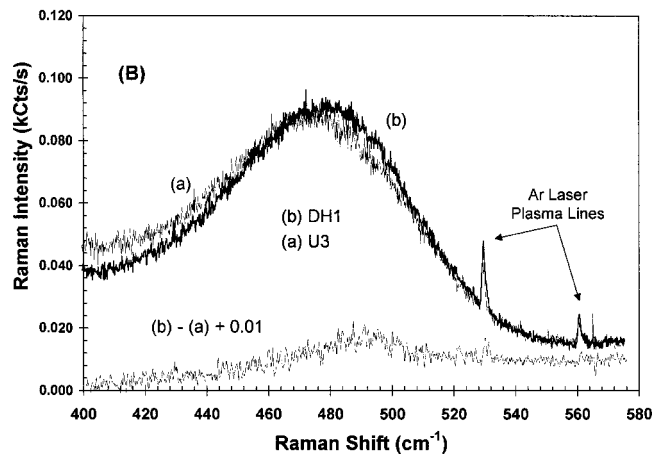
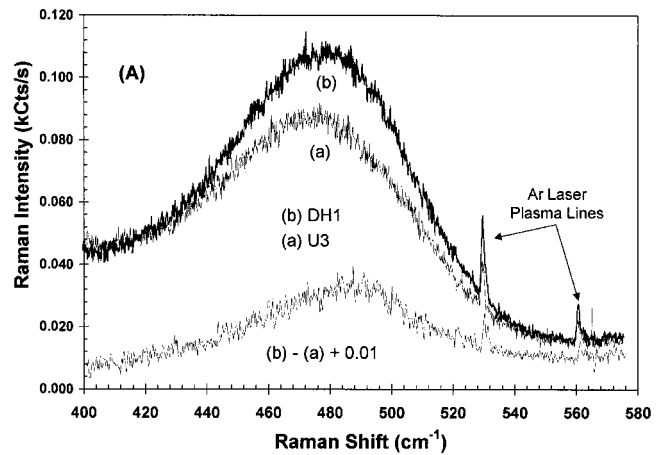


FIG. 5. Difference Raman spectra between reference (U3) sample and modified (DH1) sample with different normalization conditions, either at (A) LO or at (B) TO positions. Excess Raman scattering centered at 490 cm^{-1} is observed in either case.

absolute Raman shifts were calibrated using the plasma lines, i.e., the two very sharp features at 529.64 and 560.80 cm^{-1} .

Considering the fact that the TEM micrographs revealed the amorphous region to be a heterogeneous mixture of the chainlike objects as well as the amorphous matrix, we subtracted the normalized Raman spectrum of an undiluted sample (U3) from those of the samples prepared with H₂ dilution. We hoped thereby to observe the Raman signature of the two structural components separately. Figures 5(A) and 5(B) show the spectral subtraction for sample DH1 using in panel (A) a normalization at $\nu = 400 \text{ cm}^{-1}$ and in panel (B) a normalization of the TO band peak. In both cases, one finds in the difference spectrum a Raman band centered at about $\nu = 490 \text{ cm}^{-1}$ and whose width is 30–40 cm^{-1} . The *same* extra Raman band, albeit of larger amplitude, appears in the difference spectra of samples DH2 and DH3. In contrast, difference spectra performed among the four undiluted reference samples (U1–U4) showed no feature above the noise level. The H₂ diluted samples DL4–DL8, prepared at the lower substrate temperature ($T_s = 150^\circ \text{C}$), showed again the extra $\nu = 490 \text{ cm}^{-1}$ Raman feature in their difference spectra. This is shown for sample DL4 in Fig. 6.

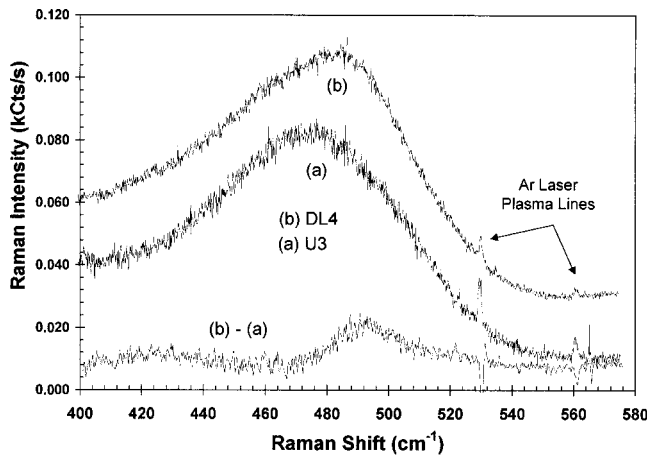


FIG. 6. Difference spectra between samples (a) U3 and (b) DL4. Traces (a) and (b) are offset for clarity.

Although the *presence* of the extra $\nu=490\text{ cm}^{-1}$ Raman band does not depend on the particular normalization procedure, the *magnitude* does, making the spectral subtraction method somewhat unreliable for the purpose of quantification. We therefore discuss two quantification methods in the Appendix.

C. Raman spectra of microcrystalline material

Figure 7 shows the Raman spectra of samples DL4–DL8 that were prepared in successively increasing H_2 dilutions at the lower substrate temperature ($T_s=150^\circ\text{C}$). The spectra show the development of the $\mu\text{c-Si}$ Raman band at $\sim 515\text{ cm}^{-1}$, as well as a distinctly evident 490 cm^{-1} band. These Raman data were also subjected to the Gaussian deconvolution analysis discussed in the Appendix. Figure 8 summarizes the relative areas of the 490 cm^{-1} band and the total microcrystalline band. The 490 cm^{-1} band already contributes an appreciable 16% of the total Raman scattering *before* the onset of the microcrystalline formation and continues to rise with H_2 dilution.

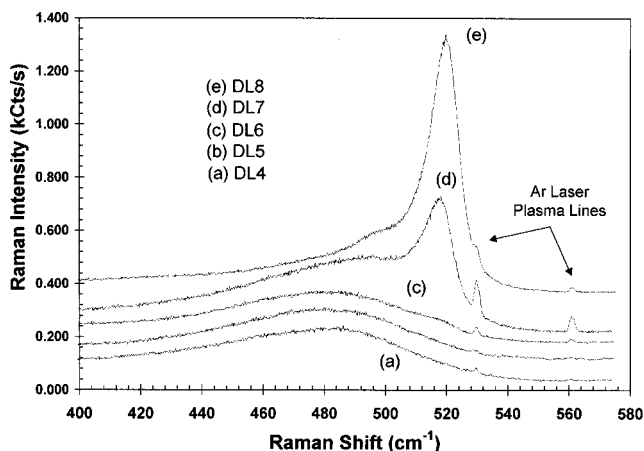


FIG. 7. Raman spectra of the very high H_2 dilution material made at a $T_s=150^\circ\text{C}$, where the H_2 dilution factor increases from samples DL4 to DL8, traces (a)–(e), respectively (see Table I).

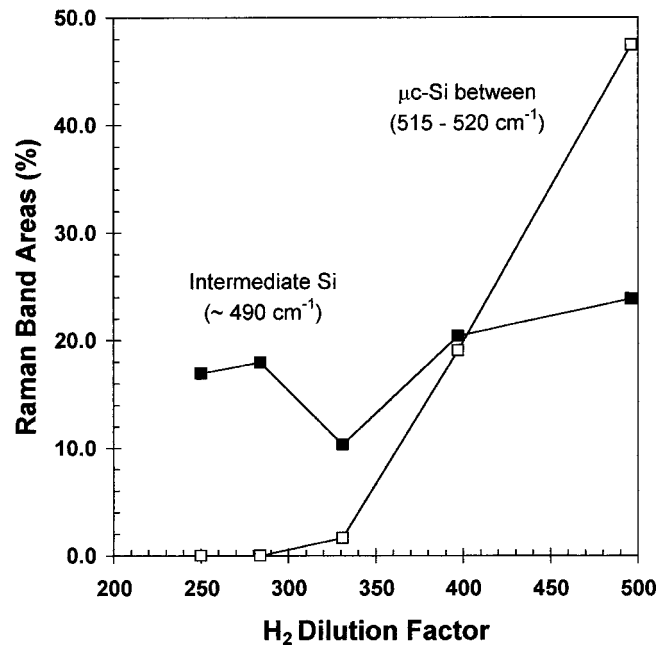


FIG. 8. Summary of the deconvolution of the Raman spectra of the DL series (very high H_2 dilution) material. The $\mu\text{c-Si}$ band area consists of the two Gaussian components required to accurately fit the feature.

IV. DISCUSSION

The TEM data reveals that heterogeneity of $a\text{-Si:H}$ involves a coexistence of chainlike structural features along with the random network of the amorphous matrix. These data differ from other forms of heterogeneity identified by others. In particular, the 2–3 nm width and up to 30 nm length of the CLO's rule out the possibility that they are related to the voids detected by low-angle x-ray scattering¹⁵ or inferred by infrared measurements.¹⁶ Their dimension also rules out any relation to polysilane (SiH_2)_n structures whose backbone and width consist of *single* Si atoms. Moreover, infrared measurements of the $a\text{-Si:H}$ films studied here show a negligible concentration of the polysilanes. Even films that show no infrared absorption of polysilane units have about 4 at. % of their hydrogen clustered and bonded to 6–8 Si atoms according to nuclear magnetic resonance studies.³ These clusters again are too small to be identified with the CLO's observed here. Moreover, the hydrogen clusters are present in essentially all $a\text{-Si:H}$ films, while the density of the CLO's is small in ordinary films, but increases with hydrogen dilution of the processing gas or with fluorination.

Our analysis of the Raman data shows that a shift of the TO peak from $\nu=475\text{ cm}^{-1}$ of the reference amorphous material to higher wave numbers with hydrogen dilution (or fluorination) (Refs. 8–10) should be interpreted as resulting from the growth in magnitude of the $\nu=490\text{ cm}^{-1}$ Raman band. Figure 8 shows that this additional Raman band is well established before the onset of microcrystallinity and is even present to a small degree in high-quality $a\text{-Si:H}$ films before H_2 dilution. Thus the 490 cm^{-1} band is *not unique* to microcrystalline material nor to the conditions in which that material is formed. The structure that causes the 490 cm^{-1} band

can be found in all hydrogenated silicon material. The difference is only in their production effectiveness, the higher the H₂ dilution level during film growth, the greater chance those structures are created.

It is noteworthy that the 490 cm⁻¹ Raman TO band is associated with high H₂ dilution levels. One of the important roles that hydrogen plays in the deposition process is an etchant role, where depositing Si atoms having high bond-strain energy are preferentially removed (etched) from the growth surface. By this etchant mechanism, a more relaxed material is produced. Thus dilution, using high levels of H₂ gas during deposition plays the same role in achieving structural relaxation as previously found⁹ by the use of fluorine. With this association, the 490 cm⁻¹ band must be related to a structural component that has reduced bond-strain energy. The improvement in the optoelectronic performance of *a*-Si:H with H₂ dilution is further evidence that the 490 cm⁻¹ TO band is connected to a relaxed structure. Reduction of the SWD has been attributed to a more ordered microstructure in *a*-Si:H films that allows the recombination of photoexcited electron-hole pairs without structural changes that result in Si dangling-bond defects.¹⁷

The Raman scattering having a TO position of 490 cm⁻¹ is clearly associated with a higher level of structural relaxation. We propose that the ordered CLO's (observed in the TEM data) are in fact those relaxed structural elements, i.e., that the Raman scattering of the CLO's have a TO band with a 490 cm⁻¹ peak position. The case for making this association can be fortified by considering the reason the TO band shifts position in silicon materials. By far, the dominant mechanism for shifting the TO peak position is by variations in strain energy.

We have assumed that the 490 cm⁻¹ Raman band does in fact represent a TO phonon vibration. This assumption is based on the following factors. Early modeling, especially the Steinhard-Alben-Weaire model,¹⁸ quite successfully modeled the radial distribution function of amorphous Si and Ge by considering the amorphous materials to be a CRN and included three features that attempt to minimize strain energy, including (1) restricting the first-neighbor bond length to vary by less than 0.1%, (2) allowing the second-neighbor distance and bond angle to vary by up to 10%, and (3) allowing odd-member ring statistics. In addition, the phonon structure of *a*-Si was theoretically obtained using the CRN framework by the use of *only two* "Keating" force constants,¹⁹ one for the bond stretching and the other for the bond-bending forces. Even with such limited use of parameters, the Keating constants can describe a wide range of structures from the crystalline state to the CRN of the amorphous state. These widely differing structures have basically the *same* phonon character because that character is rather insensitive to the environment beyond the second nearest neighbor, i.e., because their near-neighbor environments are nearly indistinguishable. However, differences in strain between these states cause the positions of the various vibrational bands, e.g., TO, LO, TA, and LA bands, to shift, the difference being in the position of the bands (the most sensitive of which is the TO band) and not the character of the bands. Thus, a structure that is neither CRN nor crystalline,

but has some intermediate (i.e., other) composure, can also be expected to have the same basic phonon character for it is not possible to alter the near-neighbor environment of Si atoms in any meaningful way. Thus Raman spectroscopy is somewhat limited in its ability to deduce any further characteristics that a particular atomic arrangement might have, e.g., as in the dihedral angle dependence. It is therefore evident that the 490 cm⁻¹ band does in fact represent a TO vibration.

It is evident that deviations of the bond angle from the ideal 109.5° of tetrahedrally coordinated systems is an important factor governing the strain and thus the peak position of the TO Raman band. Having found by TEM that the CLO's are highly ordered, one is forced to conclude that they must be composed of bonding units having very little if any BAD, for even moderate levels of BAD destroys order.

The relationship between BAD and Raman TO peak position and peak width has been studied in detail.²⁰⁻²² We find that not only is our measured TO peak position of 490 cm⁻¹ consistent with a vanishing level of BAD, so is our determination of its width (from 35 to 40 cm⁻¹). Of particular interest is that model calculations²¹ showed that the linear dependence of peak position and width did not continue below a BAD~4°, but tends to flatten out to a width of ~33 cm⁻¹ for BAD approaching zero. In addition, it was shown^{23,24} that as the BAD→0°, the Raman TO width→33 cm⁻¹, and the TO peak position extrapolates to ~487.5 cm⁻¹. Thus, our experimentally determined values of the TO peak position and width, of 490 and 37 cm⁻¹, respectively, are entirely consistent with those early theoretical predictions of *strain-free* phonon behavior.

The close agreement in position and width of the 490 cm⁻¹ TO band with those of the model calculations support our view that this TO band is associated with a structure that is more ordered and relaxed than what the amorphous matrix could ever be. Since the amorphous matrix is primarily a CRN, and since CRN's have a minimum BAD of ~10°, the TO band of CRN's can never rise above ~475 cm⁻¹. [We have shown that any shift in the measured (composite) peak position above this is a result of a growth in scattering strength of the 490 cm⁻¹ TO band.]

We are left with two quite independent pieces of experimental data showing the existence of regions having extremely low levels of bond-angle distortion. On the one hand, the 490 cm⁻¹ Raman TO band reveals a BAD approaching 0°. On the other hand, the TEM data reveal that the CLO's contain a high degree of order along their length. The achievement of this order is quite inconsistent with the finite levels of BAD found in the CRN structure. Thus, this too reveals the presence of regions containing very low levels of BAD. It is therefore natural to assign these two together, i.e., to conclude that the CLO's have a TO phonon of 490 cm⁻¹. So the three (and only three) structures revealed by TEM, i.e., the CRN amorphous network, the CLO's and the microcrystallites, have three distinct Raman signatures in the 475 cm⁻¹, 490 cm⁻¹, and 508–522 cm⁻¹ scattering, respectively. The intermediacy of the CLO order is not just one of range, since their length can be as large as the largest microcrystallite cluster. Nor is it just one of intermediate Raman

TO frequency. It also includes one of dimensionality, the CLO's being quasi-one-dimensional.

It is evident that the high-quality a -Si:H material used in the production of solar cells having superior photoelectronic performance, especially in regard to the SWD effect, has elevated levels of CLO's and high levels of 490 cm^{-1} Raman scattering. We propose that this enhanced performance is a result of the intermediate order of the CLO's, which are essentially strain-free. With this sort of heterogeneity, an a -Si:H film can reach an overall more relaxed state than it could if it were composed of a homogeneous amorphous matrix. Moreover, this sort of heterogeneity, comprised of the CRN and the quasilinear CLO components, should offer few interfacial defects, compared to (say) the CRN and the rather rigid three-dimensional microcrystalline structure.

V. CONCLUSIONS

Amorphous hydrogenated silicon of improved quality for photovoltaic devices can be prepared by hydrogen dilution of the processing gas. This increase in quality, as measured, for example, by a decrease in the Staebler-Wronski degradation, is accompanied by an increase in the concentration of the chainlike objects in TEM micrographs. These CLO's are quasi-one-dimensional, having 2–3-nm widths and lengths of ~ 30 nm or more. Significantly, they show a high degree of order *along* their length, implying very low levels of bond-angle distortion ($\sim 0^\circ$). We associate these with a TO Raman band at 490 cm^{-1} with a full width of $37 \pm 3\text{ cm}^{-1}$; they also independently imply vanishing levels of bond-angle distortion. Intermediate order is revealed not only by its TO peak position being intermediate in frequency between those of the CRN amorphous matrix (475 cm^{-1}) and the smallest microcrystallites ($\sim 508\text{ cm}^{-1}$), but also by the fact that the CLO's are ordered along their length compared to the zero- and three-dimensional orders of the CRN and crystalline conditions, respectively.

APPENDIX

In order to quantify the Raman spectra, we examine two different methods, both of which rely on the use of Gaussian functions: (A) Gaussian construction and (B) Gaussian deconvolution. In subsection A, we simulate the observed shifts in peak position and narrowing of the TO band by a construction of two Gaussian functions. This is done to make a historical connection between those two (position and width) commonly measured Raman parameters. In subsection B, the full Raman trace is fitted by performing a Gaussian deconvolution of the actual data.

In order to create traces that more closely resemble the measured shape of the Raman spectrum of a -Si:H, it is common practice to broaden the calculated c -Si vibrational density of states (v -DOS) by convolution with a Gaussian function.²⁵ A simplified description of the v -DOS can be had based on four Gaussian functions for the TA, LA, LO, and TO bands. This simplification is especially appropriate, however, for the crystalline TO v -DOS (our primary interest) since it is quite narrow ($\sim 30\text{ cm}^{-1}$) and intense, i.e., Gaussian-like, compared to the neighboring LO band. Since

the convolution of two Gaussians is also purely Gaussian, we expect that the convolution of the sharp (Gaussian-like) crystalline TO band with the broadening Gaussian to very closely approximate *just one* Gaussian function. This one Gaussian then represents an amorphous phase. Therefore, if the material contains multiple distinct phases, where each is represented by a distinct *level of strain*, each phase may contribute one Gaussian to the measured TO band in this description.

In the following analyses, we make use of *two* Gaussians to describe the TO Raman band. The justification for this is ultimately based on two fundamental experimental observations: (1) the spectral differences for all the H_2 diluted samples have their peaks at the same location and have \sim the same full widths, i.e., 490 and $35\text{--}40\text{ cm}^{-1}$, respectively, and (2) the TEM shows the existence of two structural components (not including the obvious microcrystallites), i.e., the amorphous matrix and the CLO's. We thus interpret the observed TO band to be a composite of two sub-bands: a primary band at 475 cm^{-1} and a secondary band at 490 cm^{-1} .

A. Quantification by Gaussian construction

In this section, we examine the changes in the peak position and full width of the composite (i.e., measured) TO band and relate these changes to differences in relative magnitudes of the two subbands. The primary Gaussian represents the TO Raman band of a -Si:H made without H_2 dilution. Its peak position and full width are taken directly from the experimental data, i.e., 475 and 70.5 cm^{-1} , respectively. As is standard practice in the field,^{10,22} the full width at half maximum is taken to be twice the half-width on the high-frequency side of the band. This is to avoid interference with the LO band centered near 400 cm^{-1} . The area of the primary band is fixed at 1. The peak position of the secondary band is fixed at 490 cm^{-1} , but its full width is not known precisely. We therefore select a few different widths from 30 to 50 cm^{-1} and for each width vary the area of the secondary band. This results in unique trajectories, in a plot of the full width versus peak position, for each secondary bandwidth. A comparison between those trajectories and the measured experimental points, shown in Fig. 9, reveals that the secondary 490 cm^{-1} band should have a full width of $\sim 35\text{ cm}^{-1}$. This is in agreement with the qualitative aspects found previously. Using this width, we thus determine the relative area of the 490 cm^{-1} band that best fits each experimental data point by minimizing the combined deviation of both the peak position and width, between the experimental and calculated values. The results are given in Table II.

B. Quantification by Gaussian deconvolution

In our deconvolution²⁶ of the experimental Raman traces, we use a *minimal* number of Gaussian functions that is consistent with the entire data set. For all of the spectra, one Gaussian is used to represent the LO band at $\sim 400\text{ cm}^{-1}$. For this band, its position, amplitude, and full width are allowed to vary during the fit. The TO band is generally represented by two Gaussians when no features due to μc -Si

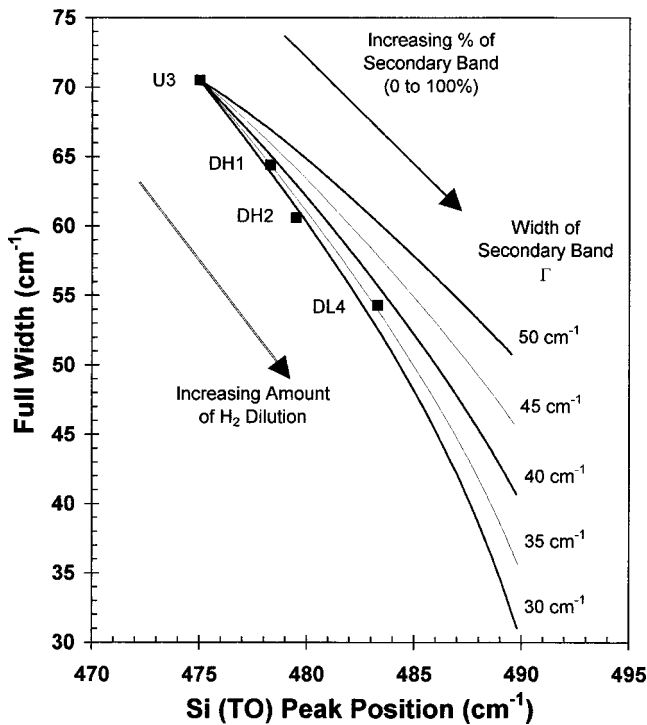


FIG. 9. Calculated relation between width and peak position of a composite curve based on the construction of two Gaussian functions, where the primary Gaussian represents the reference a -Si:H parameters taken from sample U3 and the secondary Gaussian represents the 490 cm^{-1} band vs the full width of the secondary band. Also shown are the experimental points.

material are found. In such a case when the μc -Si band is indeed observed, e.g., at $\sim 516\text{ cm}^{-1}$ for sample DH3, two additional Gaussians are required to fit that μc -Si band as one Gaussian results in a noticeably poor fit. In addition to these Raman features, two more Gaussians are used to locate the two plasma lines of the laser, which are important in establishing accurate Raman shifts.

Although one Gaussian can be used to adequately fit the TO band of the no H_2 dilution samples, one Gaussian is clearly insufficient in fitting the curves of the H_2 diluted

TABLE II. Calculated area of the secondary 490 cm^{-1} band for the samples deposited at $300\text{ }^\circ\text{C}$ by (A) Gaussian construction and (B) Gaussian deconvolution. Values are given as the percentage of the total Raman scattering.

Sample name	Secondary 490 cm^{-1} band	
	(A)	(B)
U3	0.0	4.5
DH1	4.4	10.1
DH2	7.1	9.8
DH3	12.0	15.3
DH4	13.0	18.0

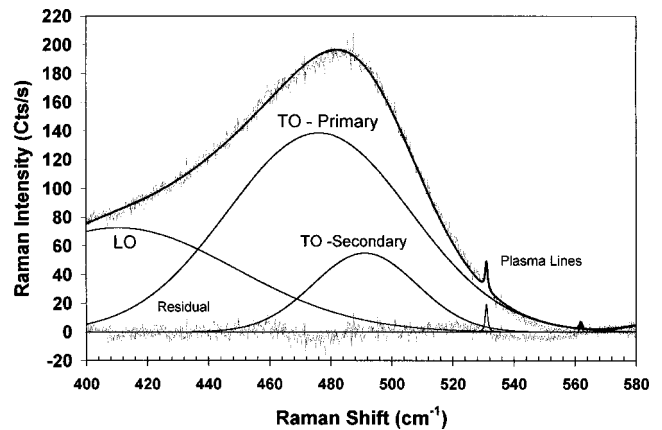


FIG. 10. Gaussian deconvolution of sample DL4 (dilution factor=250, $T_s = 150\text{ }^\circ\text{C}$).

samples. This is especially true the higher the H_2 dilution. At the other extreme, if we attempt to use three Gaussian functions to fit the TO band of the no H_2 dilution sample, we find that the amplitude of one of them always converges to zero during the fit. We therefore find that *two* Gaussians represent the minimal number that is consistent with the entire data set. The two Gaussians then represent two distinct environments within the material containing different levels of strain.

In performing multiple (m) Gaussian fits to a particular data set, there are $3m$ different parameters that can be varied, representing for each function its peak position, amplitude, and width. However, it is not our intent to minimize the resulting fit quality (χ^2) at all costs, but rather to restrict as much as possible the parameters that are allowed to vary using the experimental evidence as a guideline. Experimentally, we measure the peak position and width of the TO band of the no H_2 dilution sample to be 475 and 70.5 cm^{-1} , respectively. The position and width of the primary TO Gaussian are then fixed to these values for all of the samples. The difference spectra shown in Figs. 5 and 6 demonstrate that the excess Raman activity for all of the H_2 diluted samples is centered at 490 cm^{-1} . Therefore this position is chosen for the secondary Gaussian for all of the samples. In the previous section, the width of the secondary Gaussian that best fit the data by the construction analysis was $\sim 35\text{ cm}^{-1}$. However, we find that in the deconvolution analysis, a width of 40 cm^{-1} offers a slightly better fit, which is nevertheless consistent with the qualitative observations.

For sample DH3, we find that a single Gaussian for the μc -Si feature results in a very poor fit and that two are required to adequately fit that feature. Since we have no prejudices regarding the μc -Si components in sample DH3, all six of the parameters for the two Gaussians are allowed to vary. We find that those peaks are located at frequencies of 510.2 and 517.4 cm^{-1} , where the lower-frequency band represents μc -Si particles that are smaller in dimension than those in the higher-frequency band.⁹ The need for two Gaussians therefore indicates the existence of a range in microcrystallite sizes, as already revealed by the TEM study. The

result of the fit for sample DL4 is shown in Fig. 10. Table II gives the results for the samples prepared at 300 °C, and Fig. 8 for the samples prepared at 150 °C. Table II shows by this method that even the sample made with no H₂ dilution (U3) has a finite level of scattering in the 490 cm⁻¹ band. It seems reasonable to expect that a certain amount of heterogeneity exists even in that sample. Indeed, the TEM study showed that LCO's can even be located in such samples, albeit at low concentrations. Thus, except for the ~5% offset, the two methods give quite similar results.

ACKNOWLEDGMENTS

The authors would like to thank Professor H. Fritzsche for a critical review of the manuscript and for his invaluable advice and comments. The work at United Solar Systems Corporation was supported in part by the National Renewable Energy Laboratory (NREL) under Contract No. ZAK-8-17619-09, while the work at Energy Conversion Devices was partially supported by NREL Contract No. ZAK-8-17619-18.

-
- ¹Stanford R. Ovshinsky, *J. Non-Cryst. Solids* **32**, 17 (1979); Stanford R. Ovshinsky, Rosa Young, Wolodymyr Czybatyj, and Xunming Deng, U.S. Patent No. 5,103,284, April 7, 1992.
- ²D. L. Staebler and C. R. Wronski, *Appl. Phys. Lett.* **31**, 292 (1977).
- ³J. A. Reimer and M. A. Petrich, in *Amorphous Silicon and Related Materials*, edited by H. Fritzsche (World Scientific, New Jersey, 1989), p. 3.
- ⁴R. A. Street, J. Kakalios, C. C. Tsai, and T. M. Hayes, *Phys. Rev. B* **35**, 1316 (1987).
- ⁵W. H. Zachariasen, *J. Am. Chem. Soc.* **54**, 3841 (1932).
- ⁶J. C. Yang, X. Xu, and S. Guha, in *Amorphous Silicon Technology B 1994*, edited by E. A. Schiff *et al.*, MRS Symposia Proceedings No. 336 (Materials Research Society, Pittsburgh, 1994), p. 687; also Xixiang Xu, J. C. Yang, and S. Guha, *J. Non-Cryst. Solids* **198–200**, 60 (1996).
- ⁷J. Yang, A. Banerjee, and S. Guha, *Appl. Phys. Lett.* **70**, 2975 (1997).
- ⁸R. Tsu, M. Izu, S. R. Ovshinsky, and F. H. Pollak, *Solid State Commun.* **36**, 817 (1980).
- ⁹R. Tsu, S. S. Chao, M. Izu, S. R. Ovshinsky, G. J. Jan, and F. H. Pollak, *J. Phys. (Paris), Colloq.* **C4**, 269 (1981).
- ¹⁰R. Tsu, J. Gonzalez-Hernandez, J. Doehler, and S. R. Ovshinsky, *Solid State Commun.* **46**, 79 (1983).
- ¹¹See, for example, C. C. Tsai, in *Amorphous Silicon and Related Materials*, edited by H. Fritzsche (World Scientific, Singapore, 1988), Vol. 1, p. 123.
- ¹²Cheng Wang, Ph.D. thesis, North Carolina State University, Raleigh, NC, 1991.
- ¹³D. V. Tsu, Ben Chao, S. R. Ovshinsky, S. Guha, and J. Yang, *Appl. Phys. Lett.* **71**, 1317 (1997).
- ¹⁴Toshihiro Kamei, Paul Stradins, and Akihisa Matsuda, *Appl. Phys. Lett.* **74**, 1707 (1999).
- ¹⁵D. L. Williamson, in *Amorphous Silicon Technology B 1995*, edited by M. Hack *et al.*, MRS Symposia Proceedings No. 377 (Materials Research Society, Pittsburgh, 1995), p. 251.
- ¹⁶A. H. Mahon, P. Raboisson, and R. Tsu, *Appl. Phys. Lett.* **50**, 335 (1987).
- ¹⁷S. Guha, J. Yang, D. L. Williamson, Y. Lubianiker, J. D. Cohen, and A. H. Mahan, *Appl. Phys. Lett.* **74**, 1860 (1999).
- ¹⁸P. Steinhard, R. Alben, and D. Weaire, *J. Non-Cryst. Solids* **15**, 199 (1974).
- ¹⁹P. N. Keating, *Phys. Rev.* **145**, 637 (1966).
- ²⁰J. S. Lannin, in *Hydrogenated Amorphous Silicon*, edited by J. I. Pankove, Vol. 21 of *Semiconductors and Semimetal* (Academic, New York, 1984).
- ²¹R. Tsu, J. Gonzalez-Hernandez, and F. H. Pollack, *J. Non-Cryst. Solids* **66**, 109 (1984).
- ²²D. Beeman, R. Tsu, M. F. Thorpe, *Phys. Rev. B* **32**, 874 (1985).
- ²³R. Tsu, in *Disordered Semiconductors*, edited by M. A. Kastner, G. A. Thomas, and S. R. Ovshinsky (Plenum, New York, 1987) p. 479.
- ²⁴R. Tsu, M. A. Paesler, and Dale Sayers, *J. Non-Cryst. Solids* **114**, 199 (1989).
- ²⁵M. H. Brodsky, in *Light Scattering in Solids*, edited by M. Cardona (Springer, New York, 1975), p. 205.
- ²⁶We used PeakSolve™ software by Galactic Industries, Salem, NH.